Visualization of Zeroth, Second, Fourth, Higher Order Tensors, and Invariance of Tensor Equations

R.D. Kriz[1], M. Yaman[2], M. Harting[3], and A.A. Ray[4]

Abstract   A review of second order tensor visualization methods and new methods for visualizing higher order tensors are presented. A new visualization method is introduced that demonstrates the property of mathematical invariance and arbitrary transformations associate with tensor equations. Together these visualization methods can enhance our understanding of tensors and their equations and can be insightful in the analysis and interpretation of large complex three-dimensional numerical/experimental data sets.

keyword: tensors, tensor equations, invariance, glyphs, visualization.

1   Introduction

The advent of high performance computers (HPC) has allowed researchers to model large three-dimensional (3D) physics based simulations. Physical properties predicted by these 3D simulations often yield gradients of tensor properties that can result in large 3D topological structures. These tensor properties can also be a combination of experimental and numerical results. Tensors, their gradients, tensor equations, and the resulting 3D topological structures can be sufficiently complex such that researchers can benefit from using visualization methods in the analysis and interpretation of their HPC and experimental results.

1.1 Visualization of second order tensors: a review

Several researchers have developed useful visualization methods that represent the more common second order tensors such as stress. ***YAMAN: Either you or I can do this. How about if you start it and I'll add to it.***

Haber, R.B. (1987): VCR-Movie entitled "Dynamic Crack Propagation with Step-Function Stress Loading," *Visualization in Scientific Computing*, Ed.s, B.H. McCormick, T.A. DeFanti, and M.D. Brown, published by ACM SIGGRAPH Computer Graphics, Vol 21, No. 6.

Haber, R.B. (1990): "Visualization Techniques for Engineering Mechanics," *Computing Systems in Engineering*, Vol. 1, No. 1, pp. 37-50.

Delmarcelle, T.; and Hesselink, L. (1993): "Visualization of Second Order Tensor Fields with Hyperstreamlines," *IEEE Computer Graphics & Applications*, pp. 25-33.

Moore, J.G.; S. A. Schorn, S.A.; and Moore, J. (1994), "Methods of Classical Mechanics Applied to Turbulence Stresses in a Tip Leakage Vortex," *Conference Proceedings of the ASME Gas Turbine Conference,* Houston, Texas, October, 1994, (also Turbomachinery Research Group Report No. JM/94-90).

Hesselink, L.; Delmarcelle, T.; and Helman, J.L. (1995): "Topology of Second-Order Tensor Fields," *Computers in Physics*, Vol. 9, No. 3, pp. 304-311.

Etebari, A. (2003): Development of a Virtual Scientific Visualization Environment for the Analysis of Complex Flows," (etd-02102003-133001), Electronic Thesis and Dissertation: http://scholar.lib.vt.edu/theses/, Virginia Tech, Blacksburg, Virginia.

Hashash, Y.M.A.; Yao, J.I.; and Wotring, D.C. (2003): "Glyph and hyperstreamline representation of stress and strain tensors and material constitutive response," Int. J. Numer. and Anal.. Meth. in Geomech., Vol. 27, pp 603-626.

[1] Associate Professor, Dept. of Engineering Science and Mechanics, Virginia Tech, Blacksburg, VA 24061

[2] Graduate Research Assistant, Dept. of Physics, University of Cape Town, Private Bag, Rondebosch 7700, South Africa

[3] Professor, Dept. of Physics, University of Cape Town, Private Bag, Rondebosch 7700, South Africa

[4] Graduate Research Assistant, Dept. of Computer Science, Virginia Tech, Blacksburg, VA 24061

1.2 Fundamental tensor properties

Before visualizing tensors and tensor equations, it is important to first review some of the fundamental tensor properties that will be visualized.

1.2.1 Iinvariance and arbitrary transformations

All tensor equations are *invariant* to *arbitrary* coordinate transformations. These properties can be demonstrated for two different tensor equations that define static force equilibrium. The gradient of the second order stress tensor followed by an indical contraction defines equilibrium, [Frederick and Chang, (1997)].

$$\sigma_{ji,j} = 0, \tag{1}$$

where σ_{ji} is the second order stress tensor and the subscripts, $_{ji}$, are called indices. The indice "$_{,j}$", which operates on σ_{ji}, represents a gradient of the second order stress tensor. In this case the indice, "$_{,j}$", associated with the gradient is contracted ("summed") with one of the indices on the stress tensor where the surviving "free" indice, "$_i$", is then associated with a force vector or first order tensor.
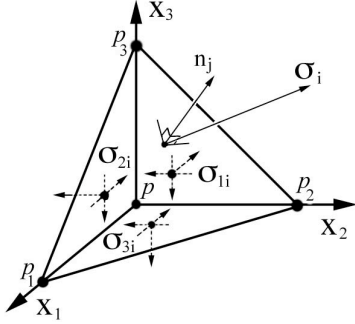

Figure 1: Equilibrium tetrahedron element where n_j is perpendicular to plane $(P_1P_2P_3)$.

The derivation of Cauchy's relation also assumes static force equilibrium.

$$\sigma_i = \sigma_{ji} n_j \tag{2}$$

where σ_{ji} is a second order tensor, σ_i is a first order stress tensor ("vector"), and n_j is a unit vector perpendicular to the plane $(P_1P_2P_3)$ on which the first order stress tensor acts, Fig.1.

Equilibrium can be visualized by using a simple free body diagram, Fig.1. The three components of the first order stress tensor, σ_i, act on plane $(P_1P_2P_3)$ and balance with the six symmetric components of the second order stress tensor, σ_{ji},

which act on the adjacent orthogonal surfaces at point P. First and second order stress tensors components exist at point P in the limit as points P_1, P_2, and P_3 approach point P [Frederick and Chang, (1972)].

The existence of static force equilibrium can be tested by *arbitrarily* transforming Eq.2 in Rectangular Cartesian Coordinates (RCC) space, x_i, where x_i transforms as a first order tensor.

$$x'_p = a_{pj} x_i \qquad \text{or} \qquad x_i = a_{pi} x'_p \tag{3}$$

Similarly, the terms in Eq.2 exist in RCC space and are tensors that transform as first and second order tensors:

$$n'_p = a_{pj} n_i \qquad \text{or} \qquad n_j = a_{pj} n'_p, \tag{4a}$$
$$\sigma'_r = a_{ri} \sigma_i \qquad \text{or} \qquad \sigma_i = a_{ri} \sigma'_i, \tag{4b}$$
$$\sigma'_{mn} = a_{mj} a_{ni} \sigma_{ji} \quad \text{or} \quad \sigma_{ji} = a_{mj} a_{ni} \sigma'_{mn}, \tag{4c}$$

where a_{ij} are direction cosine matrices (not tensors) that transform any n-th order tensor from the initial "unprimed" coordinates into the transformed "primed" coordinates. This transformation is valid for any *arbitrary* transformation. Quantities can only be labeled as an n-th order tensor if they transform as an n-th order tensor.

If Eqs.4 are substituted into Eq.2, the transformation matrices combine into Kronecker deltas, which exchange indices and the resulting equation maintains its' form ("*invariant*") but now in the transformed primed RCC system.

$$\sigma'_p = \sigma'_{qp} n'_q \tag{5}$$

Similarly Eq.1 can be transformed into the primed RCC and maintain its' form.

$$\sigma'_{ji,j} = 0 \tag{6}$$

An equation can only be called a tensor equation if each term in the equation transforms such that the equation remains unchanged ("*invariant*") and does so for any *arbitrary* transformation. The implication here is that the mathematical ideas of *invariance* and *arbitrary* transformations are consistent with our idea of a physical law. In this case the law of static force equilibrium. Where does equilibrium exist? – everywhere ("*invariant*") and does so using *arbitrary* transformation. These properties, which are inherent properties of all tensor equations, will allow us to visualize properties associated with tensor equations. It is essential that the ideas of *invariance* and *arbitrary* transformations be understood in order to grasp the idea of the visualization methods presented here. *Invariance* in a

graphical sense will be also used to visualize the *invariance* in a tensoral sense.

1.2.2 Eigenvalue-eigenvector decomposition of the second order stress tensor

For first order stress tensors, σ_i, there is one special direction for n_i where σ_i and n_i are parallel and the shear component of σ_i acting on plane $(P_1 P_2 P_3)$ is by definition zero. Such a direction is called a principal direction.

$$\sigma_i = \sigma \, n_i \tag{7}$$

For any second order stress tensor, σ_{ji} there are three mutually orthogonal directions ("eigenvectors") and their corresponding magnitudes ("eigenvalues") where the shear stress component is zero, which defines the principal stress state. Combining Eq.1 and Eq.7 yields the equation for solving for these three eigenvalues, σ, and their corresponding eigenvectors, n_i,

$$(\sigma_{ij} - \sigma \, \delta_{ij}) \, \xi_i = 0, \tag{8}$$

where n_j is rewritten as ξ_i which represents the principal stress state orientation shown in Fig.2.

The three eigenvalues (σ_a, σ_b, σ_c) are often envisioned as an ellipsoid whose major, medium, and minor axes represent the largest, intermediate and smallest magnitudes of the three eigenvalues and the orientation of this ellipsoid represent the eigenvector direction cosines, ξ_i, of a principal stress state. This ellipsoid will be referred to as the *stress ellipsoid*.

$$A_1 x^2 + A_2 y^2 + A_3 z^2 + A_4 xy + A_5 xz + A_6 yz +$$
$$A_7 x + A_8 y + A_9 z + A_0 = 0 \tag{9}$$

Although Eq.9 is not a tensor equation, it is none-the-less useful for visualization of principal stress states, but the link between graphical *invariance* and mathematical *invariance* does not exist.

2.1 Stress Quadric Surface

A second order symmetric tensor can be represented with ellipsoids by means of two entirely different methods. The eigenvalue-eigenvector decomposition, previously described, has been more commonly used to visualize stress as a *stress ellipsoid*. There is yet another ellipsoid surface that can be constructed from the stress tensor; the stress quadric [Frederick and Chang, (1972)].

$$\sigma_{ij} \, \xi_i \xi_j = \pm \, k^2 \tag{10}$$

This stress quadric is a scalar tensor equation that can also be expanded into terms that fit the polynomial in Eq.9, where

$$A_0 = \pm \, k^2, \, A_1 = \sigma_{11}, \, A_2 = \sigma_{22}, \, A_3 = \sigma_{33}, \, A_4 = (\sigma_{21} + \sigma_{12}),$$
$$A_5 = (\sigma_{13} + \sigma_{31}), \, A_4 = (\sigma_{23} + \sigma_{32}) \text{ and } A_7 = A_8 = A_9 = 0 \tag{11}$$

Hence the stress quadric is a tensor equation that also becomes a closed surface ellipsoid and is called the *stress quadric surface*.
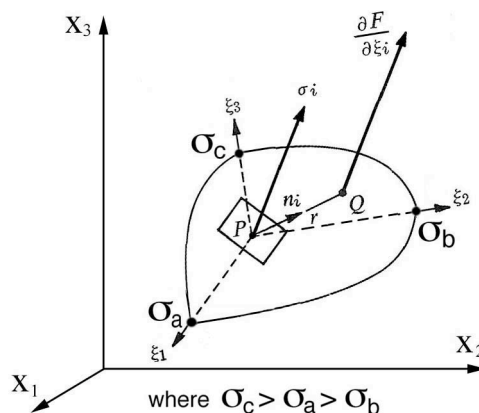

Figure 2: *Stress quadric surface at P is aligned along the principal axes, ξ_i, and shows only a portion of the ellipsoid.*

In Fig.2 point P is the same point P in Fig.1 where both σ_i and σ_{ij} coexist and the plane in Fig.2 is the same plane $(P_1 P_2 P_3)$ in Fig.1. Unlike the *stress ellipsoid*, the *stress quadric surface* has two properties of importance in visualizing the state of stress [Frederick and Chang, (1972)]:

1. Let P be the center of the ellipsoid and Q be any point on the *stress quadric surface* and the distance $PQ = r$. The normal stress at P, acting in the direction PQ is inversely proportional to r^2.

2. The stress vector, σ_i, acting across the area of plane that is normal to PQ, is parallel to the line, $\partial F/\partial \xi_i$, which acts normal to the *stress quadric surface* at Q.

The first property is exactly the inverse of the more commonly used *stress ellipsoid* and consequently the shape of the *stress quadric surface* can be intuitively misleading; the square of the length of the principal axes are inversely proportional to the principal stresses, whereas the *stress ellipsoid* visually represents the largest eigenvalue along the major principle axis and the smallest along the minor axis.

The second property visualizes all possible orientations of the first order stress tensor. All line segments that are normal to the *stress quadric surface* at point Q are also parallel to the

first order stress tensor acting at point P, on a plane pointing in the direction n_i which intersects the stress quadric surface at point Q, whereas the line segments acting normal to the *stress ellipsoid* surface have no physical significance. Unlike the *stress ellipsoid*, the *stress quadric surface* is also a tensor equation and enjoys the property of *invariance* and *arbitrary* transformations. Here the *arbitrary* transformation can be visualized as the collection of all line segments acting normal to the *stress quadric surfaces*.

Based on these observations a new visualization method is proposed that uses the more intuitive shape of the *stress ellipsoid* to visualize the principal stress state, but also allows the second property of the stress quadric to be visualized as an *arbitrary* transformation of the first order stress tensor.

2.2 A new method: visualization of stress quadric normal and shear components mapped onto the stress ellipsoid

In Fig.2 the first order stress tensor, σ_i, can be resolved into two components; 1) normal components acting parallel to n_i, and 2) shear components acting parallel to the plane. The orientation of large shear stresses can be an important factor in predicting stress-induced deformations and crack propagation. The eigenvalue-eigenvector decomposition of any second order stress tensor is a transformation where the principal axes, ξ_i, represent directions where the shearing stress is zero. Therefore the orientation of nonzero shear stresses would exist somewhere in between the principal axes, ξ_i. On the *stress quadric surface* pure shear would be viewed as line segments normal to this surface but at the same time acting parallel to the plane at point P. All these line segments would however be difficult to visualize, so the angle between σ_i and the unit normal, n_i, at point P is represented as a color at point Q. This color would represent the components of normal and shearing stress at point P by an angle, which is calculated using the *stress quadric surface*, but mapped as color onto the *stress ellipsoid* surface at point Q. Hence all of the components of the first order stress tensor, σ_j, in any *arbitrary* direction, n_i, can be visualized as a color which is mapped onto the *stress ellipsoid* surface that represents the principal stress state of σ_{ij}.

Let P be the center of the ellipsoid and Q be any point on the *stress ellipsoid* surface. The direction cosines of PQ are

$$n_i = \xi_i / r, \tag{12}$$

where $r = |PQ|$. The stress vector, σ_i, in this direction is given by Eq.2 and the angle between the unit normal, n_i, to the plane and the stress vector, σ_j, acting on that plane is calculated using the scalar product of the stress vector, σ_i, and n_i.

$$\theta = \cos^{-1}\{\sigma_i\, n_i\ /\ |\sigma_i|\} \tag{13}$$
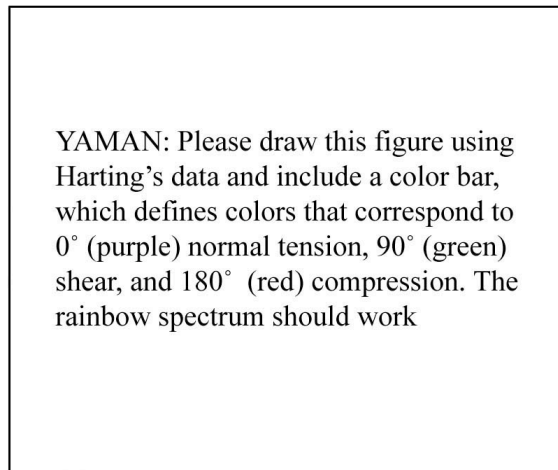
Figure 3: Color map of normal and shear stress on a *stress ellipsoid* where data was taken from [Harting, (1998)].

This angle can now be mapped as a color on a *stress ellipsoid* surface, where n_i intersects this surface at point Q. Using a standard rainbow color spectrum 0 (purple) corresponds to pure tension, 90 (green) to pure shear, and 180 (red) to pure compression. The shearing stress is visualized as green bands of color traversing the ellipsoid surface, Fig.3. This technique can be used to observe shear stress of stress tensors that were calculated from experimental data of a shot peened material [Harting, (1998)].

2   Visualization of stress gradients

Visualization of second order stress tensors can be envisioned by drawing a collection of evenly space *stress ellipsoids* or *stress quadric surfaces* in RCC space. Either of these closed ellipsoidal surfaces are referred to as a "glyph". The center glyph is used as the reference glyph and the surrounding glyphs are located at evenly spaced distances, $\pm\Delta x$, $\pm\Delta y$, and $\pm\Delta z$, which would be seen as a collection of glyphs located to the north, south, east, west, front, and back of the center glyph, Fig.4.

If the glyph spacing is small but the 3D collection of glyphs does not obscure the viewer from seeing how glyphs change their shape and orientation, than the viewer is seeing the stress gradient as a discrete change in space.

$$\Delta\sigma_{ij} / \Delta x_k \tag{14}$$

In the limit as Δx_k goes to zero Eq.14 reduces to

$$\sigma_{ij,k}, \tag{15}$$

which transforms as a third order tensor. Summing forces requires a contraction on "$_i$" and "$_k$" indices which yields,

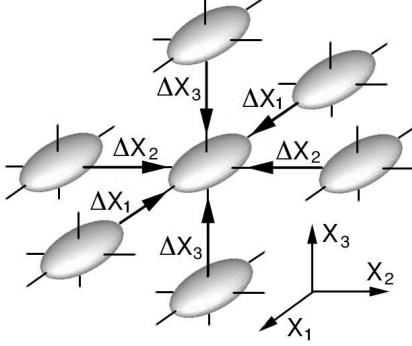$$\sigma_{kj,k}. \tag{16}$$

Figure 4: Stress glyph gradient where there is no change in shape or orientation of the nearest neighboring stress glyphs.

Comparing Eq.16 with Eq.1 suggests that it may be possible to see the stress state of static force equilibrium, but only if the viewer can visually confirm that Eq.16 does indeed sum to zero, on indice "$_k$". Stress glyphs shown in Fig.4 are all the same therefore the gradient, $\sigma_{ij,k}$, is indeed zero. If the stress glyphs surrounding the center glyph all have different shapes and orientations than it is debatable if the observer can envision how the summation, $\sigma_{kj,k}$, goes to zero. However any gradient in Fig.4 does indeed visually represent force equilibrium but only in the limit as Δx_k goes to zero. This limiting process could be more accurately envisioned as changes in the surrounding glyphs' shape, color and orientation as they collapse onto the center glyph from any *arbitrary* direction. Such a collection of glyphs would visually represent the gradient in any *arbitrary* direction.

Because it is difficult to properly envision this limiting process graphically using discrete glyphs, early research on visualization of tensor tubes, allowed the viewer to envision gradients, but only in one direction, [Delmarcelle and Hesselink (1995)]. For example take a series of stack glyphs in the X_3 direction, Fig.5, but remove the σ_c component of the glyph and scale this eigenvalue as color, which is mapped onto the circumference of the remaining two-dimensional (2D) ellipse and then connect all possible colored 2D ellipses into a "tensor-tube". Now extend this idea in all possible directions. What would this graphical image look like? One possible implementation of this idea is to envision a 3D stress glyph disturbance emanating from a point source, similar to Huygen's principle for 2D plane waves, but using 3D stress quadric glyphs instead. This is an interesting idea, but very difficult to visualize. One immediate requirement would be that, although this surface maybe irregular, it must be symmetric to satisfy equilibrium and its' gradient.
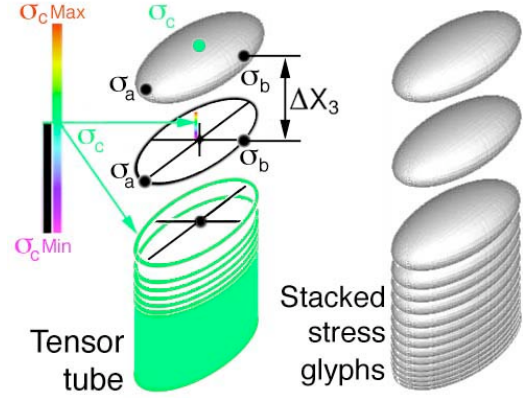

Figure 5: Stacked stress glyphs and tensor tubes

Although stress glyphs are seen to occupy space, like scalar quantities, stress glyphs represent properties that exist at points. But unlike scalar quantities second order stress tensors are not invariant it arbitrary RCC transformations. Recall quadric stress ellipsoids are visual representations of all possible transformations at a point, therefore stress glyphs become a graphical *invariant* at that point. Of course stress glyphs will change from point to point and so the graphical idea of *invariance* at points extends to their 3D stress gradient structures shown in Fig.4 and Fig.5. Hence there is a link between graphical and tensor equation *invariance* not just at points but through out RCC space.

4 Visualizing fourth order stiffness tensors

Here our objective is to look at a spherical disturbance such as a dilatational pulse, which initially expands equally in all directions. Invoking Huygen's principal the reader can envision very small 2D plane waves, which exist on the surface of a very small sphere in the center of an anisotropic crystal. Each of these plane waves travels in a specific direction called the pointing vector, ν_i, at a speed that corresponds to elastic properties in the same direction. Hence, plane waves traveling in different directions in an anisotropic material will travel at different speeds and the continuous collection of all of these plane waves, although initially a sphere, soon deviates into a nonspherical shape simply because plane waves will travel faster in stiffer directions and slower in less stiff directions.

First we start with the equations of motion for a continuum.

$$\sigma_{ji,j} = \rho \ \partial^2 u_i / \partial t^2 \tag{17}$$

where ρ is the material density and u_i is the displacement. Recall Hooke's law for an anisotropic material,

$$\sigma_{ij} = C_{ijkl} \ l_{kl}, \tag{18}$$

and substitute the strain-displacement relationship,

$$l_{ij} = (u_{i,j} + u_{j,i}) / 2 \qquad (19)$$

into to Eq.18 yields

$$\sigma_{ij} = C_{ijkl} \, u_{k,l} \qquad (20)$$

Substituting Eq.20 into Eq.17 yields the equation of motion in terms of displacements.

$$\partial \,(C_{ijkl}\, u_{k,l}) / \partial \, x_j = \rho \;\; \partial^{\,2}\, u_i / \partial \, t^2 \qquad (21)$$

This equation is further reduced if the material is assumed to be homogeneous, $\partial \, C_{ijkl} / \partial \, x_j = 0$. Next assumed a plane wave periodic disturbance for the displacement, u_k, which is written in exponential form.

$$u_k = A \; \alpha_k \; e^{\,i\,k\,(\nu_i\, x_i - v\, t)} \qquad (22)$$

where v is the wave velocity, k is the plane wave number, ν_i is the propagation direction ("pointing vector"), and α_k is the particle vibration directions. Substituting Eq.22 into Eq.21, reduces to an eigenvalue problem.

$$(\, C_{ijkl} \; \nu_j \; \nu_l - \rho v^2 \, \delta_{ik} \,) \; \alpha_k = 0 \qquad (23)$$

This is called the Christofel's equation of motion. If Eq.23 is expanded into a 3 by 3 matrix, it is perhaps easier to see that the velocity terms along the diagonal, ρv^2, are eigenvalues and the displacement direction cosines, α_k, are eigenvectors.

Closer examination of Eq.23 reveals that along a prescribed propagation direction, ν_j, both the eigenvalues and eigenvectors can only be functions of the fourth order stiffness tensor, C_{ijkl}. If the eigenvalues (wave speeds) are calculated for all possible propagation directions, ν_i, this would generate a 3D wave velocity surface for each eigenvalue. Since there are three eigenvalues, Eq.23 predicts three wave velocity surfaces. The eigenvectors, which are particle vibration direction cosines, can be mapped onto eigenvalue surfaces as color at the point where ν_i intersects the wave surface. Color is defined by the cosine of the angle, $\alpha_k \nu_k$, separating two unit vectors. Hence color visually defines the eigenvector (vibration direction), α_k, with respect to the propagation direction, ν_k: $\alpha_k \nu_k = 0$ (pure longitudinal) and $\alpha_k \nu_k = 1$ (pure transverse). Using the rainbow color spectrum, color would reveal the wave type: 1) pure longitudinal, 0˚ or purple, 2) pure transverse, 90˚ or red,

and 3) a mode transition, 45˚ or green which would indicate a transition from longitudinal to transverse. With colors the observer can quickly determine the wave type and discover locations of possible mode transitions.
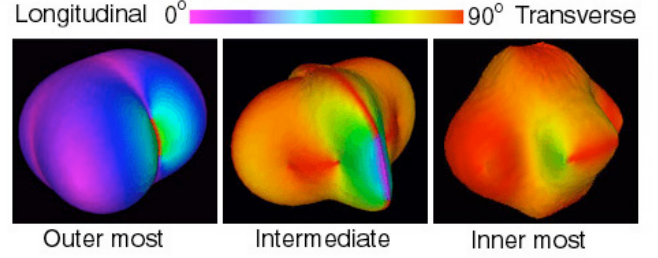

Figure 6: Wave velocity (eigenvalue) surfaces for Calcium-Formate, where color is the wave-type which is defined by the cosine of the angle, $\alpha_k \nu_k$, separating two unit vectors: the vibration direction (eigenvector), α_k, with respect to propagation direction, ν_k.

Together the three surfaces, shown separately in Fig.6 or connected in Fig.7, uniquely represent the fourth order elastic stiffness tensor, C_{ijkl}, at a point.
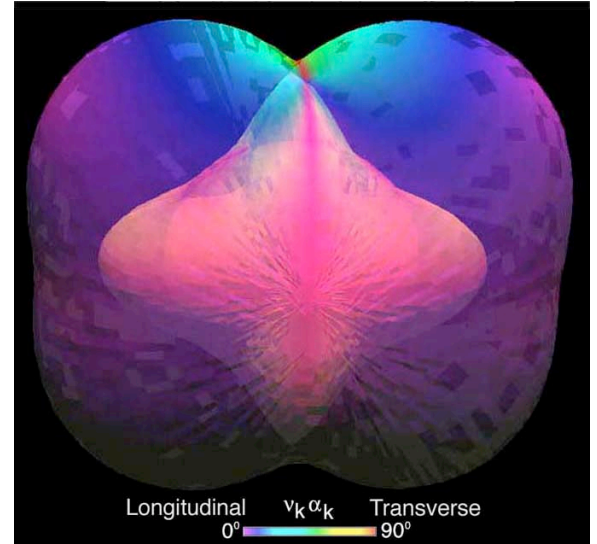

Figure 7: Combined wave velocity surface for Calcium-Formate where translucent outer surfaces show a single connected surface, C_{ijkl} [Ledbeter and Kriz (1992)].

Wave velocity surfaces are drawn for a highly anisotropic orthorhombic crystal called Calcium-Formate, $Ca[HCOO]_2$, Fig.6. Because of its' unusual orthorhombic anisotropy, this particular symmetry results in a single connected surface, Fig.7, [Kriz and Ledbetter (1982)]. These geometries are now being used as new sub-classification scheme within orthorhombic symmetry, [Musgrave (1982)].

The concept of second order stress tensor gradients was presented in section 4 as a discrete event showing how the shape and orientation of stress glyphs change as they collapse onto a center stress glyph. But extending this concept as a continuous gradient in all directions was difficult to envision, but perhaps could be approached as a dilatational pulse. The derivation Eq.23 assumed such a dilatational pulse, so perhaps Eq.23 and Eq.8, which are both eigenvalue problems, are related. It is easily shown that there are only two free indices in the first term of Eq.23, which can than be rewritten as a second order tensor, β_{kl}, and the scalar term, ρv^2, can be rewritten as, β, and substituted back into Eq.23,

$$(\beta_{kl} - \beta\, \delta_{kl})\, \alpha_k = 0 \qquad (24)$$

where Eq.24 and Eq.8 have the same ("*invariant*") form. This supports the proposed idea that a continuous stress gradient in all directions is equivalent to a dynamic dilatational pulse and therefore the images ("glyphs") shown in Fig.7 which represent the fourth order stiffness tensor, C_{ijkl}, are related to the gradient of a second order stress tensor, $\sigma_{ji,k}$, Fig. 4, but in a continuous sense in all directions.

3 Visualizing zeroth order tensors and their tensor equation invariance

Scalar variables are zeroth order tensors, which are the easiest tensor quantities to visualize. By definition scalar quantities are invariant to any arbitrary coordinate transformation at a point but can change value at adjacent points. This is the simplest idea of a gradient.

$$\vec{\nabla} F(x,T,t) = \frac{\partial F(x,T,t)}{\partial x}\vec{i} + \frac{\partial F(x,T,t)}{\partial T}\vec{j} + \frac{\partial F(x,T,t)}{\partial t}\vec{k} \qquad (25)$$
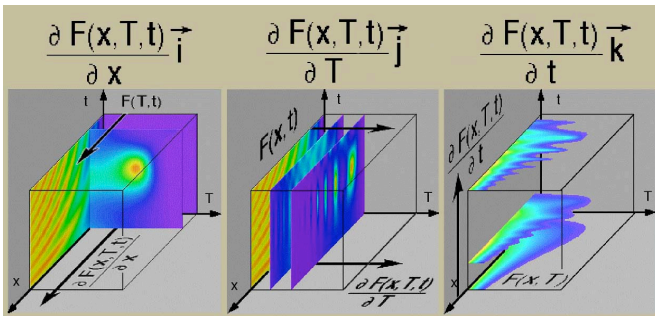

Figure 8: Gradients of a scalar function in parametric space and its' visual analog.

Gradients of scalar functions can be visualized by moving orthogonal planes through a region of interest where color patterns within the moving plane change as a plane moves along one of the three independent axes, Fig.8. Gradients in

Fig.8 demonstrate a visual analog to the mathematical gradient operator on a scalar function, F(x,T,t), [Kriz, (1991)].

Gradients of a scalar function can also be visualized by using a translucent voxel volume element, which can map an entire 3D region as a single continuous function, Fig.9. These gradients are best viewed by a smooth and continuous rotation [Kriz, Glaessgen, MacRae, (1997)]. This rotating image provides a comparative format similar to Tufte's comparison of "Tables and Graphs", where simple graphs are superior as a comparative format but lack the quantitative format required by scientific analysis or engineering design, [Tufte, (1990)]. The effect of rotating voxel volume imaging in some cases yields dramatic results, especially when the function is continuous with several contrasting regions.
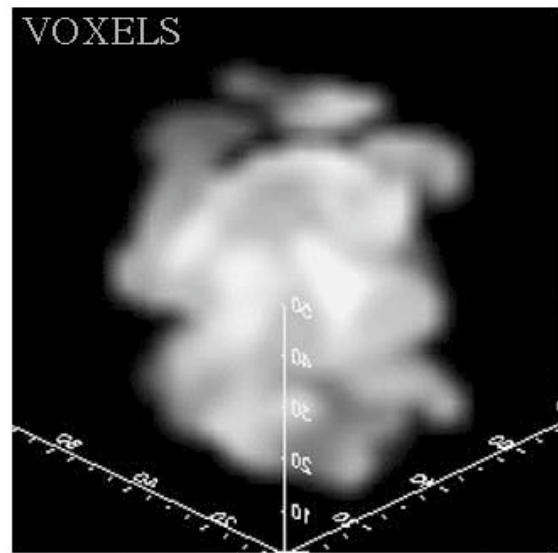

Figure 9: Translucent voxels show a continuous gas-air gradation, [Brown and Boris, (1990)], where the 3D gradient is viewed when rotated [Kriz, Glaessgen, MacRae, (1997)].

Rotating voxel images demonstrate the cognitive analytic power of the mind: that is, even elaborate and expensive computer tomography systems cannot accomplish the same numerical reconstruction of a 3D-volume with the same speed. Indeed our minds are capable of reconstructing a 3D gradient instantaneously over the entire volume. This example is one of the best examples of the analytic power of visual thinking [Kriz, Glaessgen, MacRae (1997)].

Scalar quantities are also visualized using isosurfaces. In Fig.10 only one ("iso") value 50% of a gas-air mixture is shown as an isosurface. This isosurface creates a 3D structure, which is a more quantitative measure of the gas-air mixture. It would be possible to show this surface growing or shrinking as the gas-air percentage is increased or decreased respectively. Isosurface movement is another method used to visualize a gradient but this only works for

small fluctuations at one particular value of the isosurface.

Often there is more than one scalar function. For example, pressure and temperature can simultaneously exist within the same RCC space. With new graphical features it is possible to extend the previous visual methods to observe how multiple scalar functions share the same parametric space and can also be used to test for the existence of new functional relationships.
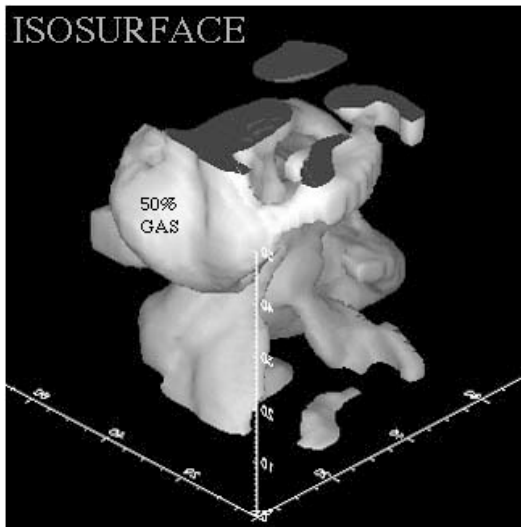

Figure 10: Volume visualization of the same gas-air gradation in Fig.9 but using isosurfaces at a mixture of 50%.

The new visual method is developed in terms of multiple parameters, which are defined either as independent or dependent parameters. For example visualizing the scalar function in Fig.8 is a four parameter model where the scalar function, F(x,T,t), is the dependent parameter and parameters x, T, and t are the three remaining independent parameters that are visualized as coordinate axes. The new method allows for n-dependent parameters and m-independent parameters, but for simplicity only a seven parameter (n=3, m=4) model will be developed here as an example.

In the following example seven parameters will be visualized where four of the seven parameters are chosen as independent variables (not necessarily RCC space) and the three remaining parameters are scalar functions that share that parametric space. This example is shown in Fig.11 where the first three parameters (P1, P2, P3) are independent variables, shown here as orthogonal axes, and the fourth orthogonal parameter is reserved as another independent variable that exists uniformly the same everywhere, but which can not be drawn as an axis: i.e. P4 = time (the fourth orthogonal axis that can not be shown). Because the three dependent parameters are functions that share the same independent parametric space, only three of which can be seen, this method provides a common basis from which to test for the existence of relationships between these three

functions. In this example it is important to note the difference between the dependent parameters (P5,P6,P7), which are functions of P1, P2, P3, and P4, and the functional relationship between the P5, P6, and P7 functions.

The visual task is to find the functional relationship between P5, P6, and P7, if any exists. The key idea here is that not all independent parameters have to be visually represented as coordinates, but can be varied independently through an interactive graphical interface such as a dial or slider.

At some arbitrary point in Fig.11 each scalar function has a unique value: e.g. P5 = 80, P6 = 120, and P7 = 220, Fig.11. Units are intentionally not shown. Obviously these values can change at adjacent points. This is our idea of a gradient. Although it is not possible to see all possible values for all three functions in the same region, it is possible to see an isosurface for each function as a separate shaded surface that intersect at a common but arbitrary point. If the observer can interactively change the isosurface value in Fig.11 and instantaneously observe the corresponding change in shape, then a gradient near this point could be determined for each function, but only in that immediate region. For example if the scalar property were fluid pressure it would be possible to envision the direction of flow.
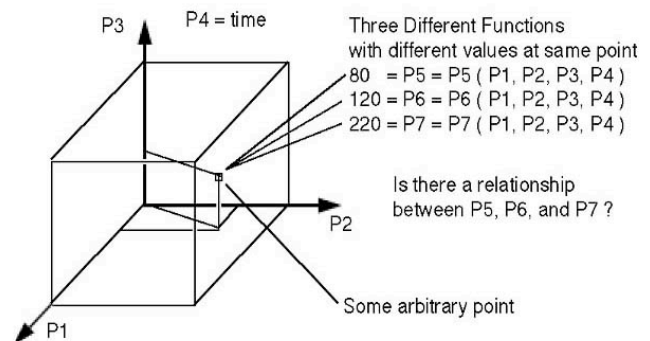

Figure 11: General parametric space (P1,P2,P3,P4) with three arbitrary dependent parameter (P5,P6,P7) functions.

Although it is highly recommended to think of the physics as a visual method is used to analyze a data set, the visual method is first developed only with respect to the property of mathematical *invariance*. Hence this visual method is generalized and can be used for any arbitrary set of scalar functions (dependent parameters) that share a common basis. A 3D data set without units is presented here where two of the three dependent parameters are drawn as unique but intersecting isosurfaces in Fig.12. If the surfaces do not intersect then it is not possible to determine a functional relationship between P5, P6, and P7. If the surfaces intersect, then there is an opportunity to investigate if this functional relationship is linearly proportional or inversely proportional.

It is not necessary to determine the functional form of each dependent parameter P5, P6, and P7 by a curve fitting

method. In fact the functional relationship between P5, P6, and P7 can be determined without knowing anything about the dependent parameter functions. Many data sets are generated by experimental scanning or numerical simulations and lack a functional form to begin with. Curve fitting these dependent parameter functions is avoided and our attention focuses on how these arbitrary shapes (arbitrary functions) relate only to each other.

If the three dependent parameters are arbitrarily chosen as spherical functions, then P5 and P6 can be conveniently viewed as nonconcentric intersecting spheres in Fig.12. If P7 is antoher dependent parameter that is not related to P5 or P6, then when P7 is mapped as a color onto the P6 isosurface, color gradients would not be seen to align with the P5-P6 intersection in Fig.12. Because of the small range of colors for P7, the alignment of P7 color gradients is difficult to see on the P6 isosurface (mostly green). Therefore P7 is also represented as an isosurface, which is also seen not to align with at P5-P6 intersection and demonstrates that there can be no functional relationship between P5, P6, and P7. However, if P7 is observed as a constant color near the P5-P6 intersection as shown in Fig.13 or if the P7 isosurface intersection occurs near the P5-P6 intersection, then a simple linear functional relationship exists between P5, P6, and P7. In both Fig.12 and Fig.13 the independent parameter P4 (time) is held constant.
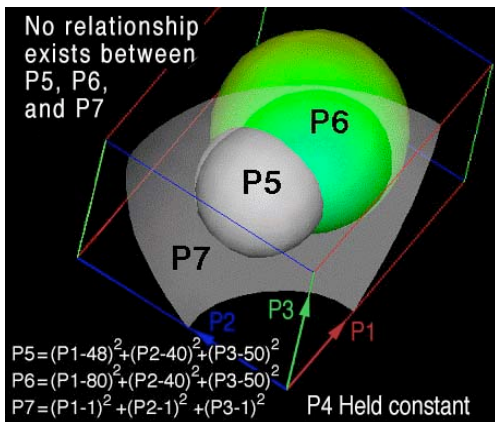

$$P5 = (P1-48)^2 + (P2-40)^2 + (P3-50)^2$$
$$P6 = (P1-80)^2 + (P2-40)^2 + (P3-50)^2$$
$$P7 = (P1-1)^2 + (P2-1)^2 + (P3-1)^2$$

P4 Held constant

Figure 12: No relationship exists between P5, P6, and P7. A translucent surface P7 is drawn intersecting the P5 and P6 isosurfaces because small changes in the P7 color gradient mapped onto the P6 isosurface is difficult to see.

Results shown in Fig.13 only confirms that a simple linear relationships exist, which could be one of three possible relationships:

P5 P6 P7 = constant,   (26)

P5 P6 = constant P7,   (27)

P5 = constant P6 P7.   (28)

These equations will be eliminated or confirmed visually.

If P6 is held fixed while the P5 isosurface is arbitrarily increased and the color or surface for P7 is observed to increase near the P5-P6 intersection, then Eq.26 is eliminated as a possible functional relationship. If P5 is held fixed while the P6 isosurface is arbitrarily increased and the color or surface for P7 is observed to decrease near the P5-P6 intersection, then Eq.27 is also eliminated as a possible functional relationship, but Eq.28 is satisfied where P4 was held constant. Finally, if parameters P5, P6, and P7 are all held fixed and only P4 is changed and if similar intersecting patterns are observed at any *arbitrary* value for P4, then the surviving functional relationship, Eq.28 is valid over the entire parametric space P1, P2, P3, and P4.
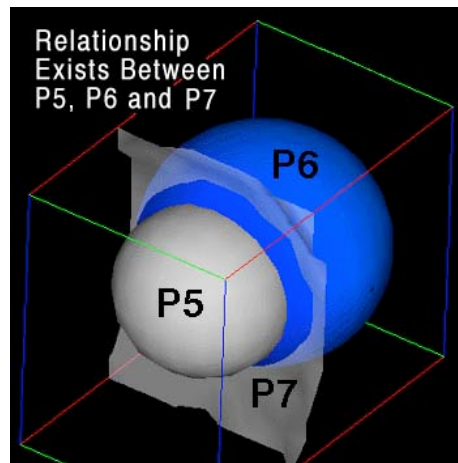

Figure 13: Simple proportional and inversely proportional relationships exist for P5, P6, and P7. P7 is rendered as a translucent isosurface, so that the observer can better view the small changes in color for the P7 property.

Here the mathematical idea of *arbitrariness* and *invariance* was used to visually confirm the existence of a tensor equation for *arbitrary* variations in dependent parameters P5, P6, and P7. In this example there are two different types of mathematical *invariance*. For Eq.28 we have a simple zeroth order tensor equation where not only are the scalar dependent parameters P5, P6, and P7 *invariant* to *arbitrary* RCC transformations at a point, but the same scalar equation itself is also *invariant* to any *arbitrary* variation that exists through out parametric space, P1, P2, P3, and P4. Both types of mathematical *invariance* are related to our idea of a physical law. That is, the parameters P5, P6, and P7 must always satisfy the same relationship independent of any *arbitrary* change that exists within parametric space P1, P2, P3, and P4. This same visual-mathematical paradigm of *invariance* can be extended to higher order tensor equations.

Simple scalar relationships, such as Eq.28, commonly occur in nature. For example let P1, P2, P3 be RCC coordinate

space and P4 = time, and let P5, P6, and P7 be pressure, P, density, ρ, and temperature, T, respectively in Fig.14 and the constant in Eq.28 becomes the gas constant, R. Where does the gas law exist? – anywhere in space (P1,P2,P3) or time (P4) and does so for any *arbitrary* variations in P5, P6, or P7.

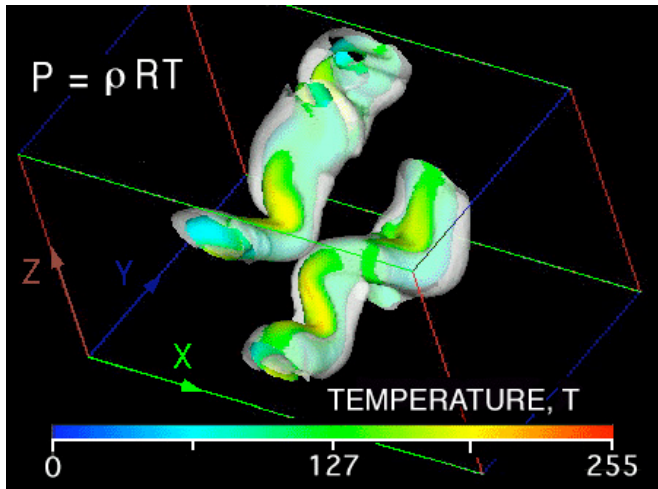$$P = \rho\, R\, T \qquad\qquad (29)$$

Figure 14: Extracting a linear zeroth order tensor equation from numerical data of a simulation where mixing occurs in a boundary layer at supersonic speeds, [Ragab and Sheen, (1990)]. Temperature is left intentionally nondimensional.

4 Summary

All graphical representations of tensor properties and functional relationships of these tensor properties in tensor equations exist at points. Although these graphical images ("glyphs") occupy space they represent properties that exist at points and like scalar quantities these properties and how they are visualized are *invariant* to *arbitrary* transformations at points and through out independent parameter space.

Again it is noteworthy that verifying the existence of simple zeroth order tensor (scalar) relationships is accomplished without determining the functions (dependent-parameters) P5, P6, and P7 in parametric space (P1, P2, P3, P4). However graphical curve fitting is required but only to visually confirm the existence of the proposed functional relationships between P5, P6, and P7. Again the idea of graphical and mathematical *invariance* is used.

Many more complex relationships can be visually extracted from raw data by using this same method. Many data sets are generated by experimental scanning or numerical simulations and lack a particular relationship to begin with. In all cases, just like finding solutions to differential equations, the researcher can guess possible relationships and then confirm them visually, because graphical and mathematical *invariance* coexist. Here we assumed simple linear

relationships. Using this method, researchers can explore large complex data sets for trends and other possible functional relationships. A graphical *invariant* pattern, associated with a relationship, is first observed then visual cognitive thought is the mechanism that allows the investigator to confirm the existence of the possible relationship. Again we use the computer to perform tedious graphical tasks where in the past only a few gifted scientists demonstrated an inherent ability to perform this same graphical process psychically.

5 References:

Federick, D.; and Chang, T.S. (1972): *Continuum Mechanics,* Scientific Publishers, Inc. Boston, pp. 38-40.

Musgrave, M.J.P., (1981): On an Elastodynamic Classification of Orthorhombic Media. *Proc. R. Soc. Lond.* A374, p. 401.

Ledbetter, H.M.; and Kriz, R.D. (1982): Elastic-Wave Surfaces in Solids. *Physica Status Solidi*, (b) Vol. 114, pg. 475.

Haber, R.B. (1987): VCR-Movie entitled Dynamic Crack Propagation with Step-Function Stress Loading. *Visualization in Scientific Computing*, B.H. McCormick, T.A. DeFanti, and M.D. Brown (eds), published by ACM SIGGRAPH Computer Graphics, vol. 21, no. 6.

Tufte, E.R. (1990): *The Visual Display of Quantitative Information*. Graphics Press, Cheshire, Connecticut.

Haber, R.B. (1990): Visualization Techniques for Engineering Mechanics," *Computing Systems in Engineering*, vol. 1, no. 1, pp. 37-50.

Ragab, S.A.; and S. Sheen, S. (1990): Numerical Simulation of a Compressible Mixing Layer. *AIAA No. 90-1669, AIAA 21st Fluid Dynamics, Plasma Dynamics and Lasers Conference.*

Kriz, R.D., (1991): Three Visual Methods. *Class notes, EMS4714, Scientific Visual Data Analysis and Multimedia*: http://www.sv.vt.edu/classes/ESM4714/ESM4714.html.

Delmarcelle, T.; and Hesselink, L. (1993): Visualization of Second Order Tensor Fields with Hyperstreamlines. *IEEE Computer Graphics & Applications*, vol. 13, no. 4, pp. 25-33.

Moore, J.G.; S. A. Schorn, S.A.; and Moore, J. (1994), Methods of Classical Mechanics Applied to Turbulence Stresses in a Tip Leakage Vortex. *Conference Proceedings of the ASME Gas Turbine Conference,* Houston, Texas, October, 1994, (also Turbomachinery Research Group Report No. JM/94-90).

Hesselink, L.; Delmarcelle, T.; and Helman, J.L. (1995): Topology of Second-Order Tensor Fields. *Computers in Physics*, vol. 9, no. 3, pp. 304-311.

Harting, M. (1998): A Seminumerical Method to Determine the Depth Profile of the Three Dimensional Residual Stress State with X-Ray Difffraction. *Acta. Meter.*, vol. 46, no.4, pp. 1427-1436.

Kriz, R.D.; Glaessgen, E.H.; and MacRae, J.D. (1995): Eigenvalue-Eigenvector Glyphs: Visualizing Zeroth, Second, Fourth and Higher Order Tensors in a Continuum. *Workshop on Modeling the Development of Residual Stresses During Thermalset Composite Curing*, University of Illinois: Champaign-Urbana, September 15-16, 1995, http://www.sv.vt.edu/NCSA_WkShp/kriz/WkShp_kriz.html.

Etebari, A. (2003): Development of a Virtual Scientific Visualization Environment for the Analysis of Complex Flows," (etd-02102003-133001), Electronic Thesis and Dissertation: http://scholar.lib.vt.edu/theses/, Virginia Tech, Blacksburg, Virginia.

Hashash, Y.M.A.; Yao, J.I.; and Wotring, D.C. (2003): Glyph and hyperstreamline representation of stress and strain tensors and material constitutive response. *Int. J. Numer. and Anal. Meth. in Geomech.*, vol. 27, pp 603-626.